Research Article

Kun Zhang* and Jiangping Cao

Dynamic behavior and modulation instability of the generalized coupled fractional nonlinear Helmholtz equation with cubic–quintic term

https://doi.org/10.1515/phys-2025-0144
received November 20, 2024; accepted March 23, 2025

Abstract: In this work, the main objective is to study the dynamic behavior of the generalized coupled fractional nonlinear Helmholtz equation with cubic–quintic term, which describes soliton propagation in nonlinear optics through the theory of dynamical system. First, the original equation is transformed into an integer-order coupled partial differential equation using Atangana's fractional derivative. Then, considering traveling wave and linear transformations, a two-dimensional planar dynamical system is constructed. Through phase portraits, stability analysis, and parameter sensitivity analysis, the dynamical behavior of the system is studied. Next, considering the dynamic behavior of the system under triangular periodic perturbation and logarithmic perturbation respectively, the reasons for the evolution of the system behavior patterns under different initial conditions are analyzed. Through qualitative analysis, we have avoided the limitations and errors of precise solution methods, and obtained the stability of the system equilibrium point under parameter changes, as well as the dynamic behavior of the system, including periodic and chaotic behaviors. Finally, by investigating the modulation instability of the system, the conditions for maintaining stability of the system are obtained through the linear stability analysis method.

Keywords: fractional derivative, chaotic behavior, cubic–quintic nonlinear effect, modulation instability

1 Introduction

As is known to all, with the flourishing development of calculus in the sixteenth century, integer-order derivative has been widely applied in fields such as physics, engineering, and biology [1–3]. But with the deepening of applications and the emergence of high-order practical problems, new tool-fractional-order derivative has emerged [4]. In 1730, Euler briefly explored the meaning of fractional-order derivative in an article and proposed the concept of fractional-order derivative. In 1812, Laplace provided a definition of fractional-order derivative through integration, further advancing the development of fractional calculus. Subsequently, Liouville formally provided the first reasonable definition of fractional-order derivative. Then, Riemann further supplemented the definition of fractional calculus. The definition of fractional-order derivative based on the Riemann–Liouville integral multiplication inverse concept proposed by him had produced profound influences on the following research in particular. Thereafter, Grünwald proposed the limiting form of fractional-order derivative, laying the foundation for another definition of fractional-order derivative. Letnikov conducted in-depth research on the definition of fractional-order derivative in limiting forms, further enriching the theoretical system of fractional-order derivative.

Due to the fact that fractional-order derivative is a derivative form between integer-order derivative and integer-order integral, it can more accurately describe nonlocal phenomena and the dynamic behavior of complex systems. Therefore, it has been applied in many fields such as signal processing, control systems, physics, biology and economics. However, fractional-order derivatives defined in different forms have different characteristics. Riemann–Liouville fractional-order derivative [5] is the earliest definition of fractional-order derivative in history and is currently a relatively well-researched fractional-order derivative in theory. It defines fractional-order derivative through a combination of integer-order derivative and integral. Caputo

* **Corresponding author: Kun Zhang,** College of Computer Science, Chengdu University, Chengdu, 610106, China; Key Laboratory of Pattern Recognition and Intelligent Information Processing of Sichuan, Chengdu University, Chengdu, 610106, China,
e-mail: zhangkun@cdu.edu.cn.
Jiangping Cao: National Institute of Measurement and Testing Technology, Chengdu, 610021, China

fractional-order derivative [6] is easier to handle initial value problems compared to Riemann–Liouville fractional-order derivative. Grünwald–Letnikov fractional-order derivative [7] is commonly used in numerical calculation, but its theoretical properties are relatively complex. Atangana's fractional derivative [8] solves the singularity problem in traditional Caputo fractional derivative, making the system continuous at the initial moment.

Researchers have constructed a variety of fractional-order differential equations when studying applied problems; they combined different types of fractional-order derivative with different equations based on problem-solving approaches. For example, the fractional-order Navier–Stokes equation [9,10] is used to describe the flow characteristics of non-Newtonian fluids. The fractional Black–Scholes equation [11] is used to depict the pricing problem of options with memory effects in financial markets. The fractional-order Fokker–Planck equation [12] is used to describe stochastic processes with fractional time derivative. Due to the different equation models established for practical problems in different fields, their characteristics are also different. With further research, the related issues of fractional-order nonlinear partial differential equation has always been a hot topic of concern. On the one hand, researchers focus on solving the problem, namely, the exact analytical solutions [13,14]. A large number of classic methods have emerged, such as Fourier transform method [15], Laplace transform method [16], Green function method [17], integral transform method [18], and special function method [19]. On the other hand, they also focus on studying the existence, stability, initial value problems, and other aspects of equation solutions without solving the antecedent problems, such as fractional-order Lyapunov method [20], Fourier spectral method [21], and operator semigroup theory [22]. In addition, with the development of computational science, there has been a heated discussion on using numerical calculation to approximate the numerical solutions of equations, such as fractional finite difference method [23], fractional variational iteration method, fractional meshless method [24], and fractional spectral collocation method [25].

We are considering using qualitative research methods for stability analysis, mainly including the use of bifurcation theory and chaos theory [26–28]. Bifurcation theory can be used to explore the occurrence and disappearance of bifurcation phenomena, the emergence and control of bifurcation instability in nonlinear systems. The bifurcation theory also has important implications for the study of chaotic phenomena, as continuous bifurcation phenomena are often a precursor to the occurrence of chaotic phenomena. By delving into the phenomenon of bifurcation, we can better understand the dynamic behavior of complex systems and provide powerful mathematical tools for solving practical problems.

In this article, we consider the generalized coupled fractional nonlinear Helmholtz equation with cubic and quintic nonlinear effects in fiber optic propagation as follows [29]:

$$\begin{aligned} &i\mathfrak{B}_t^{\alpha}u + \beta\mathfrak{B}_{tt}^{2\alpha}u + \frac{k}{2}\mathfrak{B}_{xx}^{2\alpha}u \\ &\quad + (\eta_1 |u|^2 + \eta_2 |v|^2)u + (\eta_3 |u|^4 + \eta_4 |v|^4)u = 0, \\ &i\mathfrak{B}_t^{\alpha}v + \beta\mathfrak{B}_{tt}^{2\alpha}v + \frac{k}{2}\mathfrak{B}_{xx}^{2\alpha}v \\ &\quad + (\eta_1 |u|^2 + \eta_2 |v|^2)v + (\eta_3 |u|^4 + \eta_4 |v|^4)v = 0, \end{aligned} \tag{1.1}$$

where $u = u(x, t)$ and $v = v(x, t)$ are the envelope functions. β describes the transmission characteristics of light beams in optics, and $\beta > 0$ represents the Helmholtz nonparaxial of the beam of light and reflects the interaction between the horizontal and vertical components of monochromatic light. k expresses the propagation and diffusion characteristics of light waves. η_i ($i = 1, 2, 3, 4$) are the real numbers and the coefficients of each nonlinear term, respectively; $\eta_i > 0$ and $\eta_i < 0$ describe the nonlinear terms that cause the amplitude of light waves to tend to enhance focusing or weaken diffusion during propagation. For $\alpha = \beta = k = 1$ and $\eta_3 = \eta_4 = 0$, Eq. (1.1) is transformed into the classic coupled nonlinear Helmholtz equations (CNLHE) [30]. For $\beta = 0$, we can obtain a coupled Schrödinger equation. The generalized coupled fractional nonlinear Helmholtz equation can describe more complex wave phenomena. In the traditional Helmholtz equation, it mainly describes linear, integer-order wave phenomena, such as the propagation of electromagnetic waves, and sound waves. in the uniform medium. However, in practical situations, many wave phenomena are nonlinear, and the medium may have fractional-order characteristics. Therefore, the generalized coupled fractional nonlinear Helmholtz equation can more accurately describe these phenomena, such as soliton propagation in nonlinear optics and sound wave scattering in complex media. In order to analyze Eq. (1.1), we consider using the Atangana's fractional derivative, which is defined in the following.

Definition 1.1. [31] AFD of order $\alpha \in (0, 1]$ for $g : [a, +\infty) \to \mathbb{R}$ is defined as:

$$\mathfrak{B}_x^{\alpha}[g(x)] = \lim_{\varepsilon \to 0} \frac{g(x + \varepsilon(x + \frac{1}{\Gamma(\alpha)})^{1-\alpha}) - g(x)}{\varepsilon}. \tag{1.2}$$

Theorem 1.2. [31] *Let g and h be two α-differentiable functions, satisfying $g(x)(h(x)) : [a, +\infty) \to \mathbb{R}$ and $\alpha \in (0, 1]$, and the properties can be obtained as follows*:

(*i*)
$\mathfrak{B}_x^\alpha(ag(x) + bh(x)) = a\mathfrak{B}_x^\alpha g(x) + b\mathfrak{B}_x^\alpha h(x),\ \ \forall a, b \in \mathbb{R}.$
(*ii*) $\mathfrak{B}_x^\alpha(C) = 0$, *where C is an real constant.*
(*iii*) $\mathfrak{B}_x^\alpha(g(x)\cdot h(x)) = h(x)\cdot \mathfrak{B}_x^\alpha(g(x)) + g(x)\cdot \mathfrak{B}_x^\alpha(h(x)).$
(*iv*) $\mathfrak{B}_x^\alpha\left(\frac{g(x)}{h(x)}\right) = \frac{h(x)\mathfrak{B}_x^\alpha(g(x)) - g(x)\mathfrak{B}_x^\alpha(h(x))}{h^2(x)}.$

Remark 1.1. AFD retains the nonlocality of general fractional derivative and has the property of being continuous at the initial moment, thus avoiding singularity problems. We will also use the following properties about AFD:

(1) $\mathfrak{B}_x^\alpha[g(x)] = \left(x + \frac{1}{\Gamma(\alpha)}\right)^{1-\alpha} \cdot \frac{\mathrm{d}(g(x))}{\mathrm{d}x}.$

(2) $\mathfrak{B}_{xx}^{2\alpha}[g(x)] = \mathfrak{B}_x^\alpha[\mathfrak{B}_x^\alpha g(x)] = g_{xx} \cdot \left(x + \frac{1}{\Gamma(\alpha)}\right)^{2-2\alpha}. + (1-\alpha)g_x \cdot \left(x + \frac{1}{\Gamma(\alpha)}\right)^{1-2\alpha}$

This article is organized as follows: in Section 2, the dynamic behavior of the solutions of Eq. (1.1) is discussed through 2D phase portraits and Poincaré section. Further research is conducted on the dynamic behavior and sensitivity analysis of the system under the influence of perturbations. By visualizing and plotting, the periodic, quasi-periodic, or chaotic behavior of the system under different parameter assignments is presented. In Section 3, by analyzing the interaction between nonlinearity and dispersion effects, the conditions for the system to obtain steady-state solutions are obtained. Finally, conclusion is proposed.

2 Dynamics behavior analysis

2.1 Mathematical analysis

The traveling wave transformation for Eq. (1.1) is considered as follows:

$$\begin{aligned} &u(x,t) = \varphi(\xi)e^{i\delta},\ v(x,t) = \chi(\xi)e^{i\delta},\\ &\xi = \xi(x,t) = \tau\left(\frac{1}{\alpha}\left(x + \frac{1}{\Gamma(\alpha)}\right)^\alpha - \frac{\iota}{\alpha}\left(t + \frac{1}{\Gamma(\alpha)}\right)^\alpha\right),\\ &\delta = \delta(x,t) = -\frac{\sigma}{\alpha}\left(x + \frac{1}{\Gamma(\alpha)}\right)^\alpha + \frac{\omega}{\alpha}\left(t + \frac{1}{\Gamma(\alpha)}\right)^\alpha + \gamma, \end{aligned} \tag{2.1}$$

where $i^2 = -1$, ι is the velocity of the solitary wave. $\varphi(\xi)$, and $\chi(\xi)$ are the functions about ξ, which are the amplitude components of solitary wave and determine the shape of the solitary wave.

By substituting the traveling wave transformation (2.1) into Eq. (1.1), we can obtain

$$\begin{aligned} &-2\omega\varphi - 2\beta\omega^2\varphi - k\sigma^2\varphi + i(-2\tau\iota - 4\beta\omega\tau\iota - 2k\sigma\tau)\varphi'\\ &\quad + (2\beta\tau^2\iota^2 + k\tau^2)\varphi'' + 2\eta_1\varphi^3 + 2\eta_3\varphi^5 + 2\eta_2\varphi\chi^2\\ &\quad + 2\eta_4\varphi\chi^4 = 0,\\ &-2\omega\chi - 2\beta\omega^2\chi - k\sigma^2\chi + i(-2\tau\iota - 4\beta\omega\tau\iota - 2k\sigma\tau)\chi'\\ &\quad + (2\beta\tau^2\iota^2 + k\tau^2)\chi'' + 2\eta_2\chi^3 + 2\eta_4\chi^5 + 2\eta_1\chi\varphi^2\\ &\quad + 2\eta_3\chi\varphi^4 = 0. \end{aligned} \tag{2.2}$$

Next, by making the transformation $\chi = \rho\varphi$, where $\rho \neq 0, 1$ and ρ is a real number, we can combine Eq. (2.2) and the aforementioned transformation to yield

$$\begin{aligned} &(2\beta\tau^2\iota^2 + k\tau^2)\varphi'' + i(-2\tau\iota - 4\beta\omega\tau\iota - 2k\sigma\tau)\varphi'\\ &\quad + (-2\omega - 2\beta\omega^2 - k\sigma^2)\varphi\\ &\quad + (2\eta_1 + 2\eta_2\rho^2)\varphi^3 + (2\eta_3 + 2\eta_4\rho^4)\varphi^5 = 0. \end{aligned} \tag{2.3}$$

By separating the real and imaginary parts of Eq. (2.3) and setting them to zero, respectively, we have

$$\begin{aligned} &(2\beta\tau^2\iota^2 + k\tau^2)\varphi'' + (-2\omega - 2\beta\omega^2 - k\sigma^2)\varphi\\ &\quad + (2\eta_1 + 2\eta_2\rho^2)\varphi^3 + (2\eta_3 + 2\eta_4\rho^4)\varphi^5 = 0,\\ &(-2\tau\iota - 4\beta\omega\tau\iota - 2k\sigma\tau)\varphi' = 0, \end{aligned} \tag{2.4}$$

then from the imaginary part Eq. (2.4), the relation can be obtained as follows:

$$\iota = -\frac{k\sigma}{1 + 2\beta\omega}. \tag{2.5}$$

Now, the real part equation can be simplified and organized as

$$\varphi'' = \lambda_1\varphi + \lambda_2\varphi^3 + \lambda_3\varphi^5, \tag{2.6}$$

where $\lambda_1 = \frac{2\omega + 2\beta\omega^2 + k\sigma^2}{2\beta\tau^2\iota^2 + k\tau^2}$, $\lambda_2 = -\frac{2\eta_1 + 2\eta_2\rho^2}{2\beta\tau^2\iota^2 + k\tau^2}$, $\lambda_3 = -\frac{2\eta_3 + 2\eta_4\rho^4}{2\beta\tau^2\iota^2 + k\tau^2}$, and $2\beta\tau^2\iota^2 + k\tau^2 \neq 0$

In order to understand the characteristics described by the real part equations, the stability and chaotic behavior of dynamical systems will be discussed using qualitative theory.

2.2 Dynamic behavior of system (1.1) *via* qualitative analysis

Due to the difficulty of solving nonlinear partial differential equations, even if exact analytical solutions are obtained through different methods, some data in the original system may still be lost. Qualitative analysis can be used to analyze the local or global dynamic behavior of the

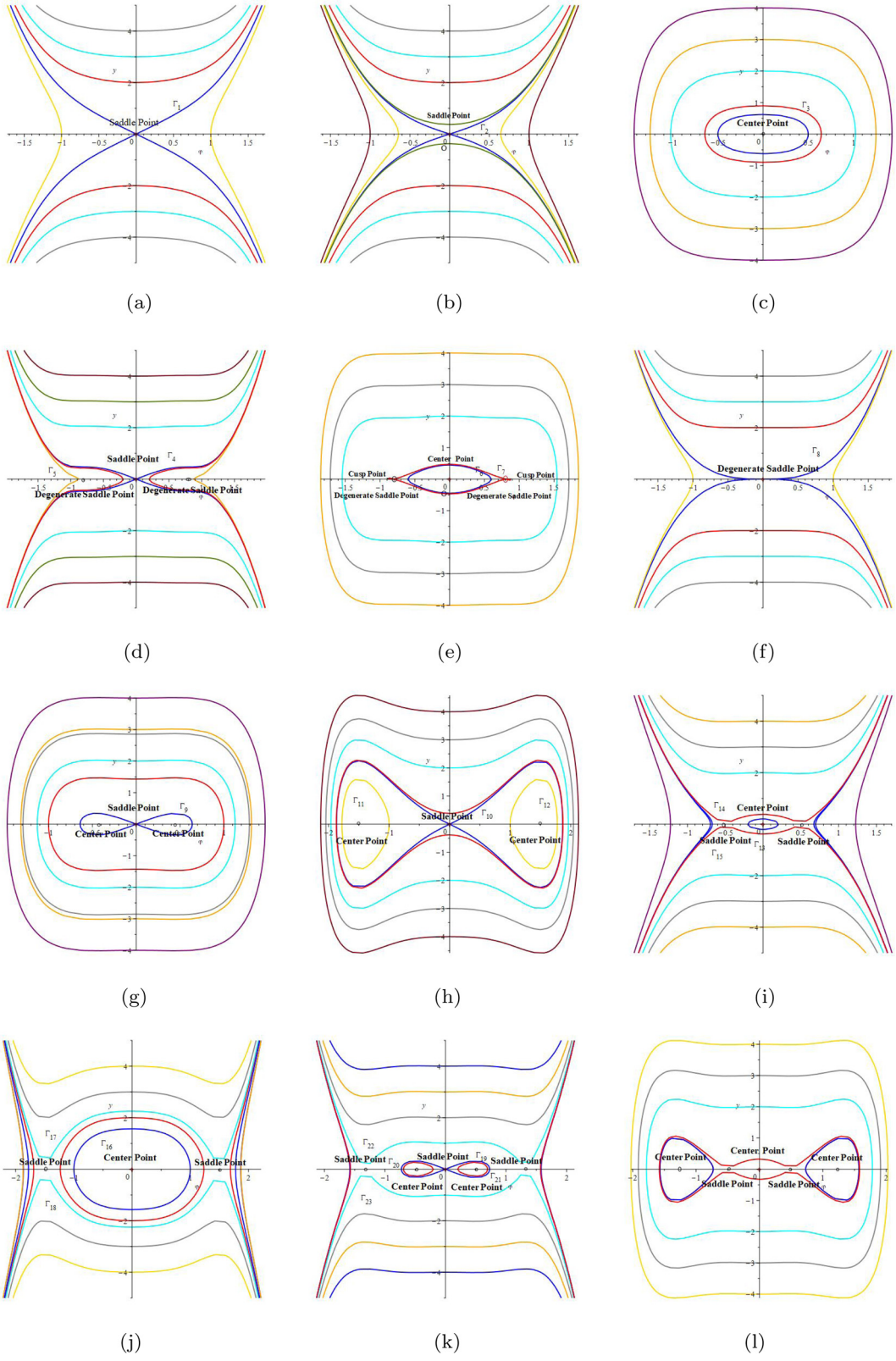

Figure 1: 2D phase portraits of system (2.7): (a) $\Delta < 0$, (b) $\Delta > 0, \lambda_1 > 0, \lambda_2 > 0, \lambda_3 > 0$, (c) $\Delta > 0, \lambda_1 < 0, \lambda_2 < 0, \lambda_3 < 0$, (d) $\Delta = 0, \lambda_1 > 0, \lambda_2 < 0, \lambda_3 > 0$, (e) $\Delta = 0, \lambda_1 < 0, \lambda_2 > 0, \lambda_3 < 0$, (f) $\Delta = 0, \lambda_1 = \lambda_2 = 0$, (g) $\Delta > 0, \lambda_1 > 0, \lambda_2 < 0, \lambda_3 < 0$, (h) $\Delta > 0, \lambda_1 > 0, \lambda_2 > 0, \lambda_3 < 0$, (i) $\Delta > 0, \lambda_1 < 0, \lambda_2 > 0, \lambda_3 > 0$, (j) $\Delta > 0, \lambda_1 < 0, \lambda_2 < 0, \lambda_3 > 0$, (k) $\Delta > 0, \lambda_1 > 0, \lambda_2 < 0, \lambda_3 > 0$, and (l) $\Delta > 0, \lambda_1 < 0, \lambda_2 > 0, \lambda_3 < 0$.

system and the sensitivity of system parameters without solving, which can comprehensively analyze the stability of the system and the existence of solutions.

Next, we convert Eq. (2.6) into a planar dynamic system:

$$\begin{cases} \dfrac{\mathrm{d}\varphi}{\mathrm{d}\xi} = y, \\ \dfrac{\mathrm{d}y}{\mathrm{d}\xi} = \lambda_1\varphi + \lambda_2\varphi^3 + \lambda_3\varphi^5, \end{cases} \tag{2.7}$$

with Hamiltonian function

$$H(\varphi, y) = \frac{1}{2}y^2 - \frac{1}{2}\lambda_1\varphi^2 - \frac{1}{4}\lambda_2\varphi^4 - \frac{1}{6}\lambda_3\varphi^6 = h, \tag{2.8}$$

where h is named the Hamiltonian constant.

At this point, we can understand the asymptotic changes of solutions and the positions of special points in the development process of dynamic systems through phase portrait and bifurcation theory.

Let $\phi(\varphi) = \lambda_1\varphi + \lambda_2\varphi^3 + \lambda_3\varphi^5 = \varphi(\lambda_1 + \lambda_2\varphi^2 + \lambda_3\varphi^4)$; thus, $\Delta = \lambda_2^2 - 4\lambda_1\lambda_3$, and $\phi'(\varphi) = \lambda_1 + 3\lambda_2\varphi^2 + 5\lambda_3\varphi^4$. Assuming that

$$J = \begin{vmatrix} 0 & 1 \\ \phi'(\varphi_i) & 0 \end{vmatrix} = -\phi'(\varphi_i) = -\lambda_1 - 3\lambda_2\varphi^2 - 5\lambda_3\varphi^4, \tag{2.9}$$

where φ_i ($i = 1, 2, 3, \ldots$) satisfies $\phi(\varphi) = 0$.

Studying the orbits and bifurcations of the planar phase portrait requires determining the special points of the system solution in the planar phase portrait, as well as analyzing the asymptotic development of the solutions under changes in system parameters. The so-called special points are the balance points of the dynamic system.

Theorem 2.1. [32] *According to the qualitative theory of the dynamic system, the equilibrium point of the dynamic system can be divided into the following three categories*:

(*i*) *If $J < 0$, then the equilibrium point $E(\varphi_i, 0)$ is the saddle point.*

(*ii*) *If $J > 0$, then the equilibrium point $E(\varphi_i, 0)$ is the center point.*

(*iii*) *If $J = 0$, then the equilibrium point $E(\varphi_i, 0)$ is the degenerate saddle point.*

There may be five equilibrium points in system (2.7), and the Hamiltonian equation at these equilibrium points is as follows: $h_1 = H(\varphi_1, 0) = 0$, $h_2 = H(\varphi_2, 0) = H(\varphi_3, 0) = \frac{12\lambda_1\lambda_2\lambda_3^2 - 2\lambda_2^3\lambda_3 + (-12\lambda_1\lambda_3^2 + 3\lambda_2^2\lambda_3)\sqrt{\Delta} - \lambda_3\Delta\sqrt{\Delta}}{48\lambda_3^3}$, $h_3 = H(\varphi_4, 0) = H(\varphi_5, 0) = \frac{12\lambda_1\lambda_2\lambda_3^2 - 2\lambda_2^3\lambda_3 + (12\lambda_1\lambda_3^2 - 3\lambda_2^2\lambda_3)\sqrt{\Delta} + \lambda_3\Delta\sqrt{\Delta}}{48\lambda_3^3}$.

According to the relationship between the roots and coefficients of system (2.7), we can obtain different phase portraits. We focus on equilibrium points and the evolution trajectories of solutions in the phase portraits, then divide the phase portraits into the following classifications.

Case 1 $\Delta < 0$ or $\Delta > 0, \lambda_1 > 0, \lambda_2 > 0, \lambda_3 > 0$ or $\Delta > 0, \lambda_1 < 0, \lambda_2 < 0, \lambda_3 < 0$.

In the event, E (0, 0) is the unique equilibrium point. When $\Delta < 0$, E (0, 0) is the saddle point, system (2.7) has a cross-track Γ_1 that passes through the saddle point; when $\Delta > 0, \lambda_1 > 0, \lambda_2 > 0, \lambda_3 > 0$, E (0, 0) is the saddle point, system (2.7) has a cross-orbit Γ_2 that passes through the saddle point. When $\Delta > 0, \lambda_1 < 0, \lambda_2 < 0, \lambda_3 < 0$, E (0, 0) is the center point, system (2.7) has a periodic closed orbit Γ_3 (Figure 1(a)–(c)).

Case 2 $\Delta = 0, \lambda_1 > 0, \lambda_2 < 0, \lambda_3 > 0$.

In this situation, system (2.7) has three equilibrium points E (0, 0) and $E\left(-\sqrt{-\frac{\lambda_2}{2\lambda_3}}, 0\right)$. $E\left(\sqrt{-\frac{\lambda_2}{2\lambda_3}}, 0\right)$. Among them, E (0, 0) is the saddle point and the others are degenerate saddle points. System (2.7) has a cross-orbit Γ_4 passing through the saddle point and a pair of nonclosed orbits Γ_5 passing through the degenerate saddle points (Figure 1(d)).

Case 3 $\Delta = 0, \lambda_1 < 0, \lambda_2 > 0, \lambda_3 < 0$.

In this case, system (2.7) has three equilibrium points E (0, 0), $E\left(-\sqrt{-\frac{\lambda_2}{2\lambda_3}}, 0\right)$, and $E\left(\sqrt{-\frac{\lambda_2}{2\lambda_3}}, 0\right)$. But unlike the second case, E (0, 0) is the center point, and the others are although degenerate saddle points. System (2.7) has a periodic closed orbit Γ_6 and a periodic closed orbit Γ_7 passing through the degenerate saddle points, which are cusp point (Figure 1(e)).

Case 4 $\Delta = 0, \lambda_1 = \lambda_2 = 0$.

In the event, system (2.7) has the unique equilibrium point E (0, 0), which is the degenerate saddle point. There are a pair of orbits Γ_8 crossing through E (0, 0). At this point, system (2.7) may have variations of increase and decrease in different directions, or may remain unchanged (Figure 1(f)).

Case 5 $\Delta > 0, \lambda_1 > 0, \lambda_2 < 0, \lambda_3 < 0$ or $\lambda_1 > 0, \lambda_2 > 0, \lambda_3 < 0$.

In this situation, system (2.7) has three equilibrium points E (0, 0), $E\left(-\sqrt{\frac{-\lambda_2 - \sqrt{\Delta}}{2\lambda_3}}, 0\right)$, and $E\left(\sqrt{\frac{-\lambda_2 - \sqrt{\Delta}}{2\lambda_3}}, 0\right)$. Among them, E (0, 0) is the saddle point and the others are center points. There have a periodic closed orbit Γ_9 (Γ_{10}) passing through E (0, 0) and a pair of periodic closed orbits Γ_{11} and Γ_{12} around the center points (Figure 1(g) and (h)).

Case 6 $\Delta > 0, \lambda_1 < 0, \lambda_2 > 0, \lambda_3 > 0$ or $\lambda_1 < 0, \lambda_2 < 0, \lambda_3 > 0$.

In this case, system (2.7) has three equilibrium points E (0, 0), $E\left(-\sqrt{\frac{-\lambda_2 + \sqrt{\Delta}}{2\lambda_3}}, 0\right)$, and $E\left(\sqrt{\frac{-\lambda_2 + \sqrt{\Delta}}{2\lambda_3}}, 0\right)$. But unlike the fifth case, E (0, 0) is the center point and the others are

saddle points. There are a periodic closed orbits Γ_{13} (Γ_{16}) and a pair of nonclosed orbits Γ_{14} and Γ_{15} (Γ_{17}, Γ_{18}) (Figure 1(i)–(j)).

Case 7 $\Delta > 0, \lambda_1 > 0, \lambda_2 < 0, \lambda_3 > 0$.

In the event, system (2.7) has five equilibrium points E (0, 0), $E\left(\pm\sqrt{\frac{-\lambda_2-\sqrt{\Delta}}{2\lambda_3}}, 0\right)$, and $E\left(\pm\sqrt{\frac{-\lambda_2+\sqrt{\Delta}}{2\lambda_3}}, 0\right)$. Among them, E (0, 0) and $E\left(\pm\sqrt{\frac{-\lambda_2+\sqrt{\Delta}}{2\lambda_3}}, 0\right)$ are saddle points and the others are center points. There are a periodic closed orbits Γ_{19} passing through E (0, 0), a pair of periodic closed orbits Γ_{20} and Γ_{21} around the center pointsm, and a pair of nonclosed orbits Γ_{22} and Γ_{23} (Figure 1(k)).

Case 8 $\Delta > 0, \lambda_1 < 0, \lambda_2 > 0, \lambda_3 < 0$.

In this situation, system (2.7) has five equilibrium points E (0, 0), $E\left(\pm\sqrt{\frac{-\lambda_2-\sqrt{\Delta}}{2\lambda_3}}, 0\right)$, and $E\left(\pm\sqrt{\frac{-\lambda_2+\sqrt{\Delta}}{2\lambda_3}}, 0\right)$. But unlike the second case, E (0, 0) and $E\left(\pm\sqrt{\frac{-\lambda_2-\sqrt{\Delta}}{2\lambda_3}}, 0\right)$ are center points and the others are saddle points (Figure 1(l)).

2.3 Perturbation analysis of system (1.1)

In practical problems, there are many small changes that affect the system. It is very meaningful to study the impact of small changes in the system on overall properties. We express small changes as a perturbation term, and when the system is based on a fundamental assumption that it is subject to small disturbances, we analyze the impact of small disturbances on the system. At the same time, the changes in system properties can be approximated by making small modifications to the original state. Next, system (2.7) with perturbation term is represented as follows:

$$\begin{cases} \dfrac{\mathrm{d}\varphi}{\mathrm{d}\xi} = y, \\ \dfrac{\mathrm{d}y}{\mathrm{d}\xi} = \lambda_1\varphi + \lambda_2\varphi^3 + \lambda_3\varphi^5 + \hbar, \end{cases} \tag{2.10}$$

where $\hbar$ is the perturbation term. We investigate the impact of different categories of perturbation terms on system (2.10).

When $\hbar = \varepsilon\cos(\mu\xi)$, where ε denotes the amplitude and μ is the frequency of the perturbation term. Specifically, this type of perturbation term is a triangular periodic perturbation term, whose amplitude and periodicity determine its small and periodic impact on system (2.10).

When $\hbar = \varepsilon\ln(1+\mu\xi)$, where ε and μ are the amplitude and the wave number of the perturbation term. Specifically, the characteristic of this perturbation term is that its amplitude changes exponentially with time or spatial position. During the propagation of optical fibers, the nonuniformity of the medium or other factors may cause the energy of the wave to decay exponentially.

Due to the different effects of different types of perturbations on the system, and the varying effects of perturbations on the system when the system parameters and initial values are different, in order to understand these characteristics, numerical calculations and visualization are used to draw 2D and 3D phase portraits with different types of perturbation terms under different parameter conditions using Maple software. In addition, since continuous systems are difficult to observe motion trajectories and analyze laws in high-dimensional situations, discretization and dimensionality reduction are performed on high-dimensional continuous systems, transforming the continuous trajectories that are originally difficult to directly observe and analyze in phase space into discrete points on the cross-section, thus simplifying the complexity of the problem. Here, the Poincaré sections are drawn, and the distribution law on the cross-section can reflect the motion characteristics of the system. Of course, considering the impact of changes in system parameters, we can also discuss sensitivity analysis of parameters and draw sensitivity analysis figures.

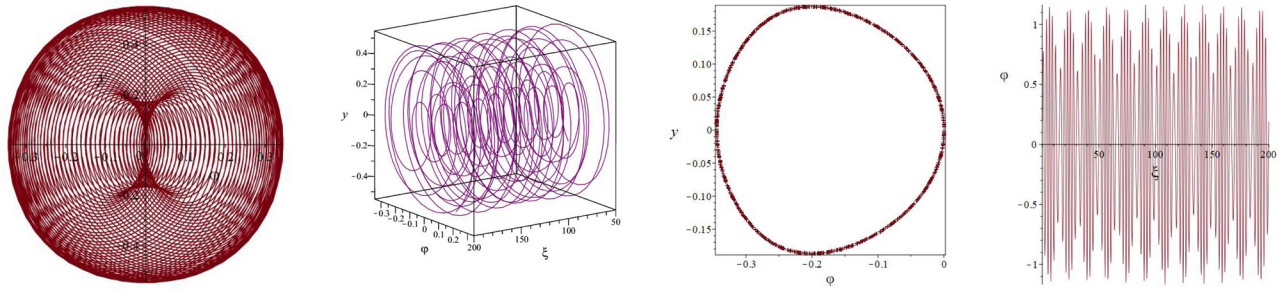

Figure 2: Perturbation analysis of system (2.10) with $\hbar = \varepsilon\cos(\mu\xi)$ for system parameters $\lambda_1 = -1$, $\lambda_2 = -4$, $\lambda_3 = -2$, $\varepsilon = 0.5$, $\mu = 2$: (a) 2D phase portrait, (b) 3D phase portrait, (c) Poincaré section, and (d) sensitivity analysis.

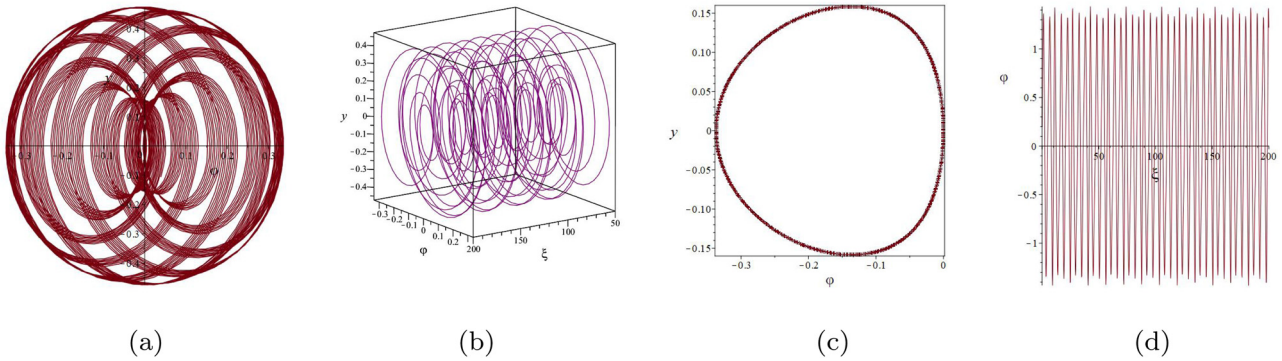

(a) (b) (c) (d)

Figure 3: Perturbation analysis of system (2.10) with $\hbar = \varepsilon\cos(\mu\xi)$ for system parameters $\lambda_1 = -1$, $\lambda_2 = 3$, $\lambda_3 = -\frac{9}{4}$, $\varepsilon = 0.5$, $\mu = 2$: (a) 2D phase portrait, (b) 3D phase portrait, (c) Poincaré section, and (d) sensitivity analysis.

When $\hbar = \varepsilon\cos(\mu\xi)$, for $\lambda_1 = -1$, $\lambda_2 = -4$, $\lambda_3 = -2$, $\varepsilon = 0.5$, and $\mu = 2$ in Figure 2, for $\lambda_1 = -1$, $\lambda_2 = 3$, $\lambda_3 = -\frac{9}{4}$, $\varepsilon = 0.5$, and $\mu = 2$ in Figure 3, for $\lambda_1 = \frac{9}{8}$, $\lambda_2 = -5$, $\lambda_3 = -2$, $\varepsilon = 0.5$, and $\mu = 2$ in Figure 4, for $\lambda_1 = \frac{9}{8}$, $\lambda_2 = 4$, $\lambda_3 = -2$, $\varepsilon = 0.5$, and $\mu = 2$ in Figure 5, for $\lambda_1 = -\frac{9}{8}$, $\lambda_2 = -4$, $\lambda_3 = 2$, $\varepsilon = 0.5$, and $\mu = 2$ in Figure 6, for $\lambda_1 = \frac{7}{8}$, $\lambda_2 = -4$, $\lambda_3 = 2$, $\varepsilon = 0.5$, and $\mu = 2$ in Figure 7, for $\lambda_1 = -\frac{7}{8}$, $\lambda_2 = 4$, $\lambda_3 = -2$, $\varepsilon = 0.5$, and $\mu = 2$ in Figure 8.

When $\hbar = \varepsilon\ln(1+\mu\xi)$, for $\lambda_1 = -1$, $\lambda_2 = -4$, $\lambda_3 = -2$, $\varepsilon = 0.3$, and $\mu = 4$ in Figure 9, for $\lambda_1 = -1$, $\lambda_2 = 3$, $\lambda_3 = -\frac{9}{4}$, $\varepsilon = 0.3$, and $\mu = 4$ in Figure 10, for $\lambda_1 = \frac{9}{8}$, $\lambda_2 = -5$, $\lambda_3 = -2$, $\varepsilon = 0.3$, and $\mu = 4$ in Figure 11, for $\lambda_1 = \frac{9}{8}$, $\lambda_2 = 4$, $\lambda_3 = -2$,

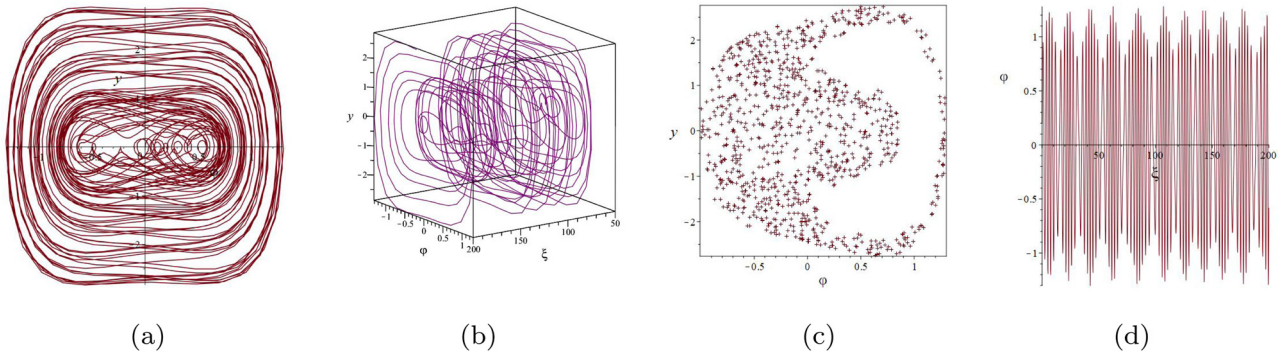

(a) (b) (c) (d)

Figure 4: Perturbation analysis of system (2.10) with $\hbar = \varepsilon\cos(\mu\xi)$ for system parameters $\lambda_1 = \frac{9}{8}$, $\lambda_2 = -5$, $\lambda_3 = -2$, $\varepsilon = 0.5$, $\mu = 2$: (a) 2D phase portrait, (b) 3D phase portrait, (c) Poincaré section, and (d) sensitivity analysis.

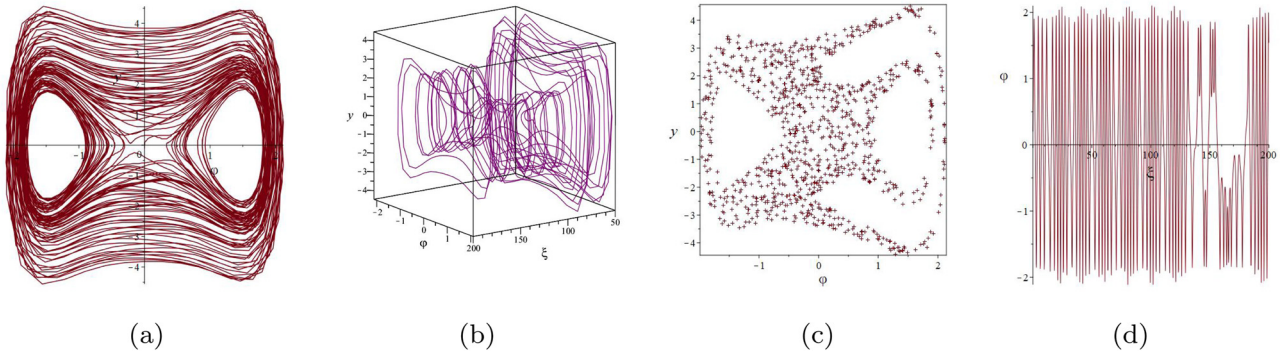

(a) (b) (c) (d)

Figure 5: Perturbation analysis of system (2.10) with $\hbar = \varepsilon\cos(\mu\xi)$ for system parameters $\lambda_1 = \frac{9}{8}$, $\lambda_2 = 4$, $\lambda_3 = -2$, $\varepsilon = 0.5$, $\mu = 2$: (a) 2D phase portrait, (b) 3D phase portrait, (c) Poincaré section, and (d) sensitivity analysis.

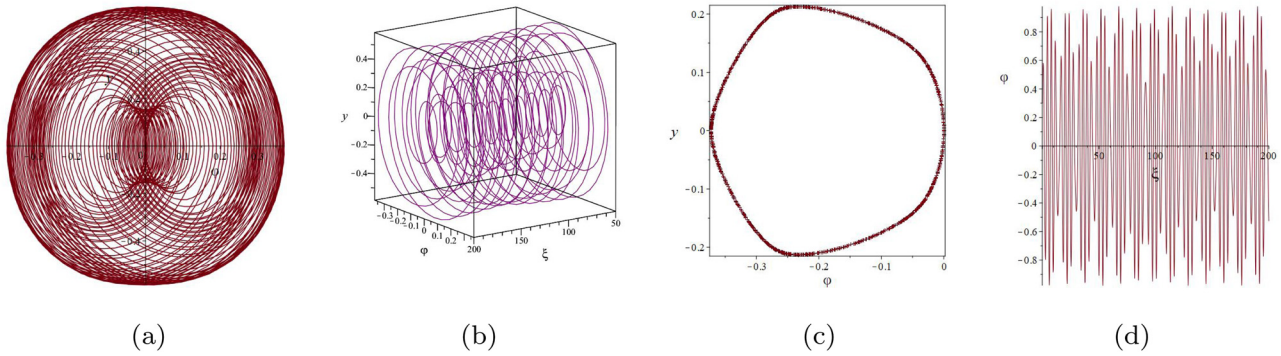

Figure 6: Perturbation analysis of system (2.10) with $\hbar = \varepsilon \cos(\mu\xi)$ for system parameters $\lambda_1 = -\frac{9}{8}$, $\lambda_2 = -4$, $\lambda_3 = 2$, $\varepsilon = 0.5$, $\mu = 2$: (a) 2D phase portrait, (b) 3D phase portrait, (c) Poincaré section, and (d) sensitivity analysis.

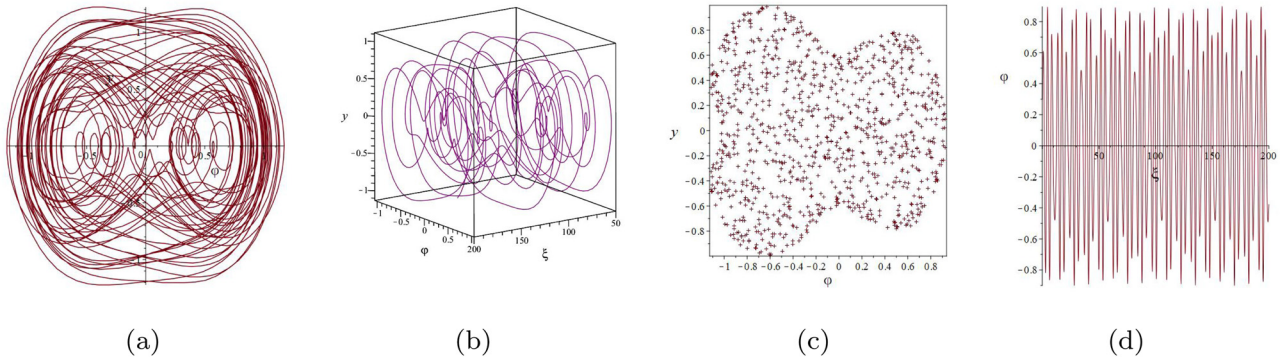

Figure 7: Perturbation analysis of system (2.10) with $\hbar = \varepsilon \cos(\mu\xi)$ for system parameters $\lambda_1 = \frac{7}{8}$, $\lambda_2 = -4$, $\lambda_3 = 2$, $\varepsilon = 0.5$, $\mu = 2$: (a) 2D phase portrait, (b) 3D phase portrait, (c) Poincaré section, and (d) sensitivity analysis.

$\varepsilon = 0.3$, and $\mu = 4$ in Figure 12, for $\lambda_1 = -\frac{9}{8}$, $\lambda_2 = -4$, $\lambda_3 = 2$, $\varepsilon = 0.3$, and $\mu = 4$ in Figure 13, for $\lambda_1 = \frac{7}{8}$, $\lambda_2 = -4$, $\lambda_3 = 2$, $\varepsilon = 0.3$, and $\mu = 4$ in Figure 14.

Through the visualization and numerical calculation, we can see that when system (2.10) is subjected to triangular periodic perturbation $\hbar = \varepsilon \cos(\mu\xi)$, under certain initial conditions, the system may exhibit periodic behavior (Figures 2, 3, 6, 8), quasi-periodic behavior (Figure 5), or chaotic behavior (Figures 4, 7). Specifically, the system exists limit-cycle, such as Figure 2. The reason for the different types of behaviors mentioned earlier is that triangular periodic perturbation may cause periodic changes in the refractive index distribution of optical fibers. The

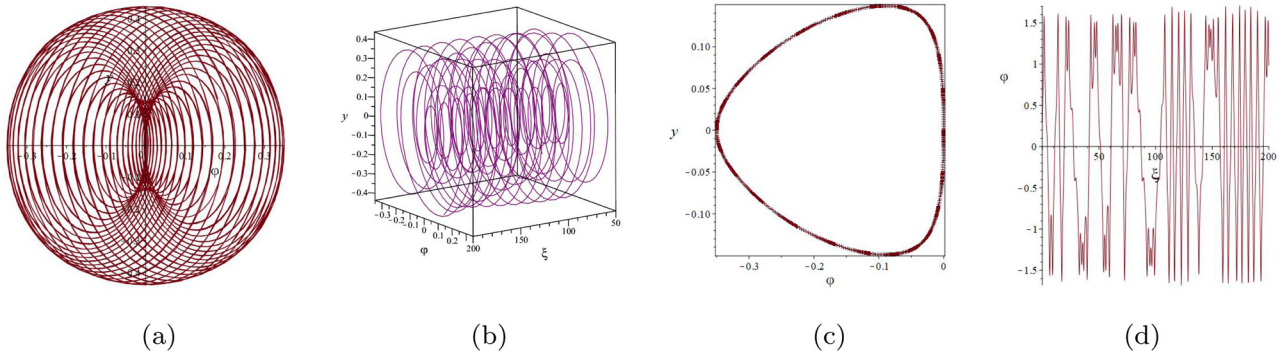

Figure 8: Perturbation analysis of system (2.10) with $\hbar = \varepsilon \cos(\mu\xi)$ for system parameters $\lambda_1 = -\frac{7}{8}$, $\lambda_2 = 4$, $\lambda_3 = -2$, $\varepsilon = 0.5$, $\mu = 2$: (a) 2D phase portrait, (b) 3D phase portrait, (c) Poincaré section, and (d) Sensitivity analysis.

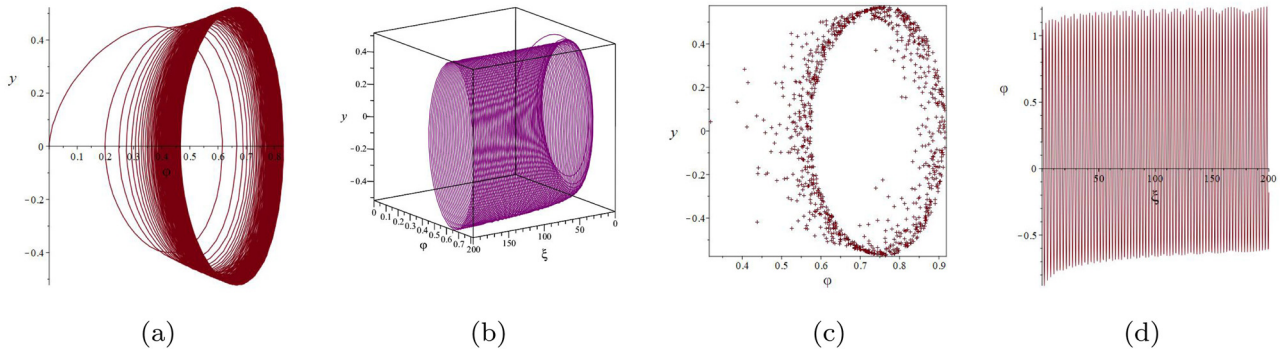

Figure 9: Perturbation analysis of system (2.10) with $\hbar = \varepsilon \ln(1 + \mu\xi)$ for system parameters $\lambda_1 = -1$, $\lambda_2 = -4$, $\lambda_3 = -2$, $\varepsilon = 0.3$, $\mu = 4$: (a) 2D phase portrait, (b) 3D phase portrait, (c) Poincaré section, and (d) sensitivity analysis.

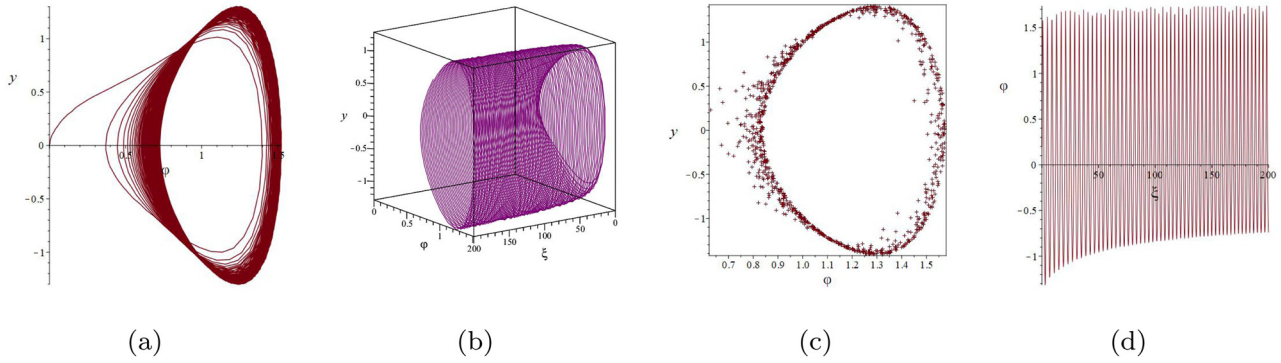

Figure 10: Perturbation analysis of system (2.10) with $\hbar = \varepsilon \ln(1 + \mu\xi)$ for system parameters $\lambda_1 = -1$, $\lambda_2 = 3$, $\lambda_3 = -\frac{9}{4}$, $\varepsilon = 0.3$, $\mu = 4$: (a) 2D phase portrait, (b) 3D phase portrait, (c) Poincaré section, and (d) sensitivity analysis.

changes will affect the transmission path and speed of light waves in optical fibers, thereby altering the phase and group velocity of optical signals. The changes in refractive index may also cause coupling between modes, leading to energy transfer and redistribution of optical signals during transmission. In addition, triangular periodic perturbations may also alter the dispersion characteristics of optical fibers, including material dispersion, waveguide dispersion, and mode-to-mode dispersion. These changes in dispersion characteristics can affect the pulse width and

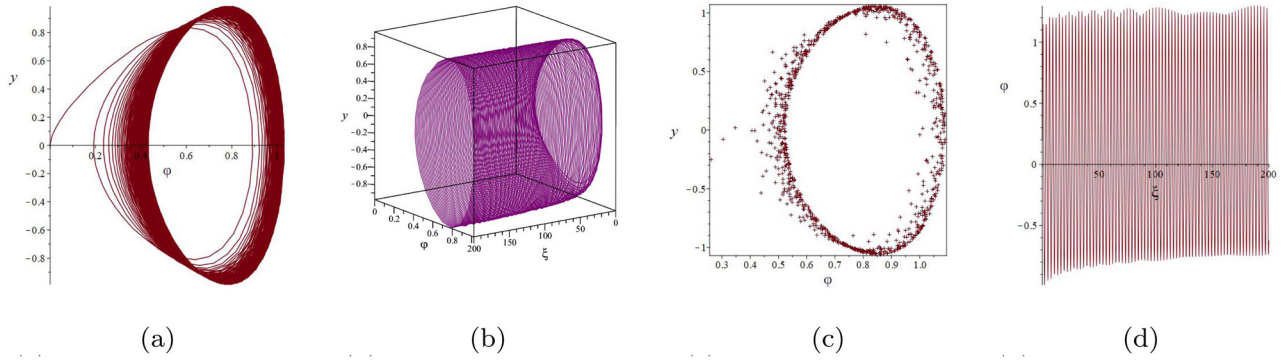

Figure 11: Perturbation analysis of system (2.10) with $\hbar = \varepsilon \ln(1 + \mu\xi)$ for system parameters $\lambda_1 = \frac{9}{8}$, $\lambda_2 = -5$, $\lambda_3 = -2$, $\varepsilon = 0.3$, $\mu = 4$: (a) 2D phase portrait, (b) 3D phase portrait, (c) Poincaré section, and (d) sensitivity analysis.

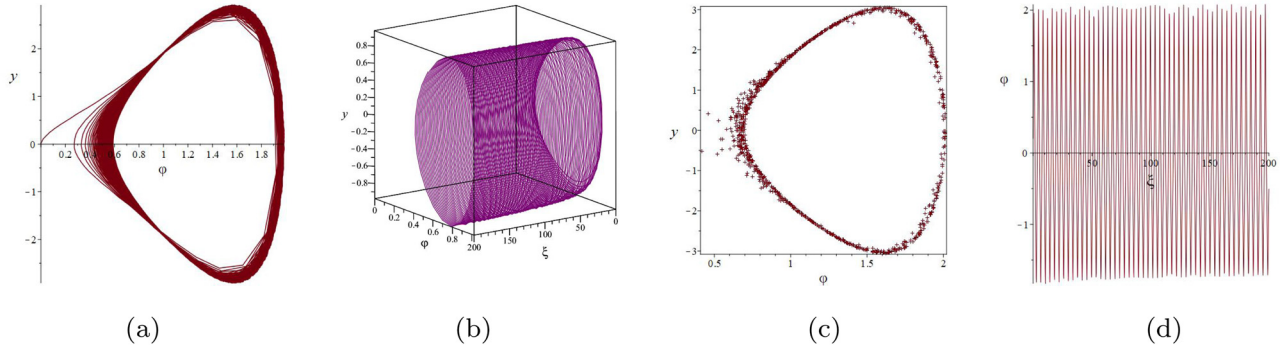

Figure 12: Perturbation analysis of system (2.10) with $\hbar = \varepsilon \ln(1 + \mu\xi)$ for system parameters $\lambda_1 = \frac{9}{8}$, $\lambda_2 = 4$, $\lambda_3 = -2$, $\varepsilon = 0.3$, $\mu = 4$: (a) 2D phase portrait, (b) 3D phase portrait, (c) Poincaré section, and (d) sensitivity analysis.

shape of optical signals, thereby affecting the transmission bandwidth and signal quality of optical fibers. When the system is affected by logarithmic perturbation $\hbar = \varepsilon \ln(1 + \mu\xi)$, due to the nonperiodicity of logarithmic perturbations and their interaction with nonlinear terms, system (2.10) exhibits chaotic behavior (Figures 9–14).

3 Modulation instability analysis

Through qualitative analysis of the dynamic behavior of Eq. (1.1), we find that optical solitons may exhibit instability during fiber propagation due to the influence of perturbations on Eq. (1.1). This instability arises from the

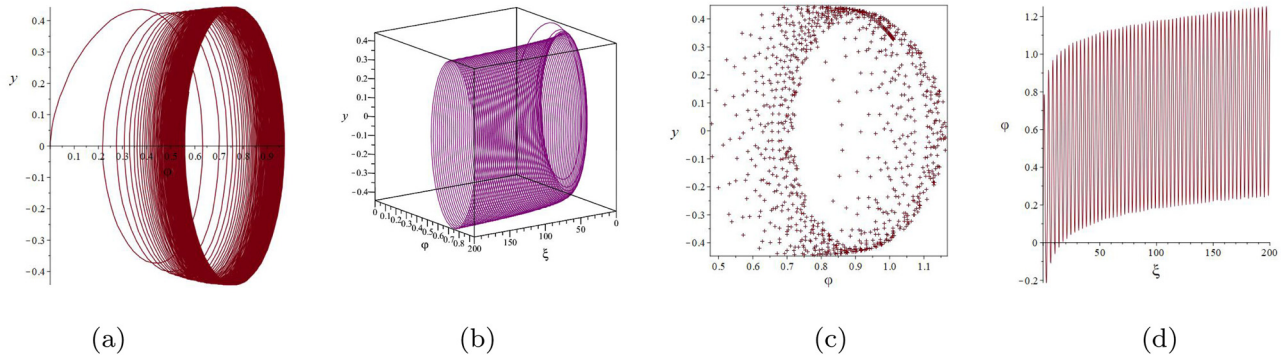

Figure 13: Perturbation analysis of system (2.10) with $\hbar = \varepsilon \ln(1 + \mu\xi)$ for system parameters $\lambda_1 = -\frac{9}{8}$, $\lambda_2 = -4$, $\lambda_3 = 2$, $\varepsilon = 0.3$, $\mu = 4$: (a) 2D phase portrait, (b) 3D phase portrait, (c) Poincaré section, and (d) sensitivity analysis.

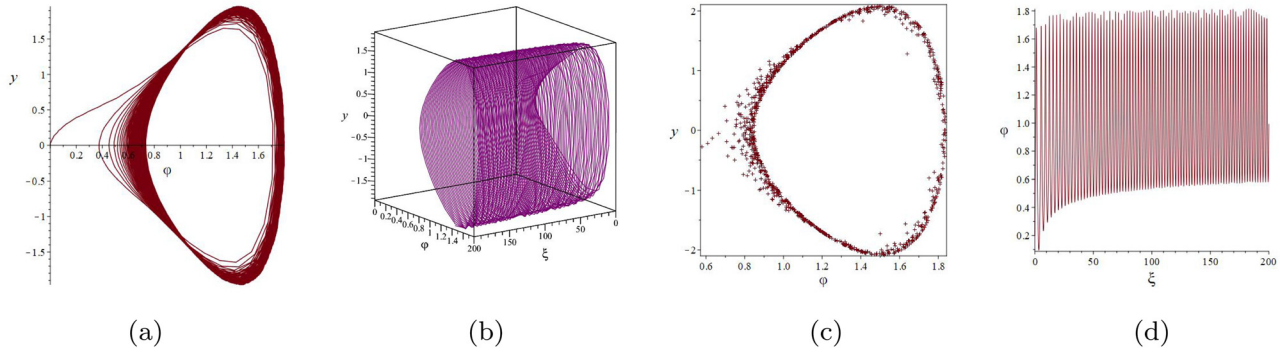

Figure 14: Perturbation analysis of system (2.10) with $\hbar = \varepsilon \ln(1 + \mu\xi)$ for system parameters $\lambda_1 = \frac{7}{8}$, $\lambda_2 = -4$, $\lambda_3 = 2$, $\varepsilon = 0.3$, $\mu = 4$: (a) 2D phase portrait, (b) 3D phase portrait, (c) Poincaré section, and (d) sensitivity analysis.

modulation effect on the steady-state caused by the interaction of nonlinear and dispersion effects.

Considering the combined effect of second-order dispersion and nonlinear effects, and taking into account the influence of perturbations, it is assumed that Eq. (1.1) has the following steady-state analytical solution $u(x,t) = (\sqrt{P_0} + q_1(x,t))e^{i\theta(x)}$, $v(x,t) = (\sqrt{P_0} + q_2(x,t))e^{i\theta(x)}$, and $\theta(x) = P_0 \varrho x$, where P_0 is input power, $\theta(x)$ denotes the nonlinear phase shift, and $q_i(x,t)$ $(i = 1,2)$ represent the perturbations. We can substitute the aforementioned expression into Eq. (1.1), and consider $q_i(x,t) = q_{\tilde{i}}(x,t), \tilde{i} = 3 - i$, $i = 1, 2$ at the same time. Taking into account both fractional derivatives and linearization, we can obtain

$$\begin{aligned} & i\left(t + \frac{1}{\Gamma(\alpha)}\right)^{1-\alpha} q_t' + \beta\left(t + \frac{1}{\Gamma(\alpha)}\right)^{2-2\alpha} q_{tt}'' \\ & + \frac{k}{2}(x + \frac{1}{\Gamma(\alpha)})^{2-2\alpha} q_{xx}'' \\ & + 3P_0(\eta_1 + \eta_2)q + 5P_0^2(\eta_3 + \eta_4)q = 0. \end{aligned} \tag{3.1}$$

From Eq. (3.1), it can be seen that the expression of perturbation $q(x,t)$ is as follows:

$$\begin{aligned} q(x,t) = {} & a_1 e^{i\left(b_1\left(x+\frac{1}{\Gamma(\alpha)}\right)^{\alpha} - b_2\left(t+\frac{1}{\Gamma(\alpha)}\right)^{\alpha}\right)} \\ & + a_2 e^{-i\left(b_1\left(x+\frac{1}{\Gamma(\alpha)}\right)^{\alpha} - b_2\left(t+\frac{1}{\Gamma(\alpha)}\right)^{\alpha}\right)}, \end{aligned} \tag{3.2}$$

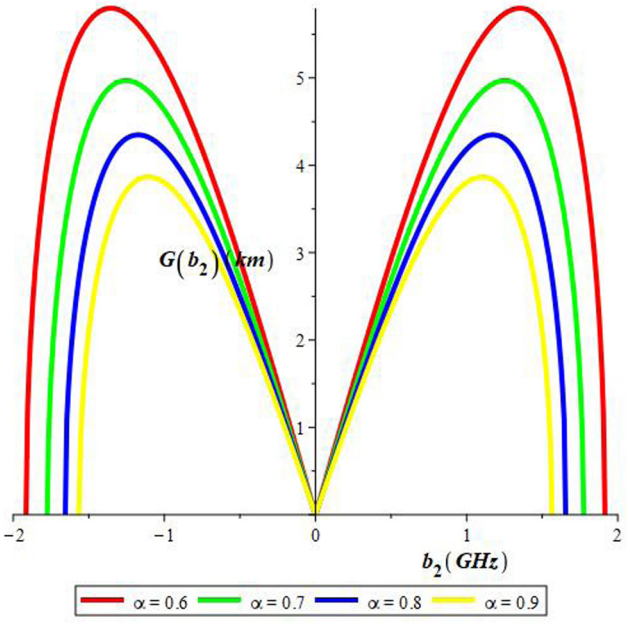

Figure 15: MI gain of $G(b_2)$ with the influence of fractional derivative order in group velocity dispersion regime for $\beta = -5ps^2/\text{km}$, $P_0 = 0.5$ W, $k = 1$, $\eta_1 = -2$, $\eta_2 = -2$, $\eta_3 = -2$, and $\eta_4 = -2$.

where a_1 and a_2 are all small parameters, and b_1 and b_2 are the wave number and frequency of the perturbation $q(x,t)$, respectively. The two terms of Eq. (3.2) represent the simultaneous occurrence of two different frequency components $\omega_0 + b_2$ and $\omega_0 - b_2$.

Eq. (3.1) and Eq. (3.2) provide two homogeneous equations about a_1 and a_2, which have nontrivial solutions when it satisfies the following dispersion relation:

$$b_1 = \pm b_2 \sqrt{-\frac{2\beta}{k} b_2^2 + \frac{6P_0(\eta_1 + \eta_2) + 10P_0^2(\eta_3 + \eta_4)}{k\alpha^2}}. \tag{3.3}$$

From the dispersion relationship of Eq. (3.3), we can obtain that the stability of steady-state solution under perturbations mainly depends on whether the transmitted beam in the fiber is in the normal dispersion region or the anomalous dispersion region.

When $\beta(3P_0(\eta_1 + \eta_2) + 5P_0^2(\eta_3 + \eta_4)) > 0$, *i.e.*, in the normal dispersion region, the steady-state solution is stable when subjected to perturbations. When $\beta(3P_0(\eta_1 + \eta_2) + 5P_0^2(\eta_3 + \eta_4)) < 0$, *i.e.*., in the anomalous dispersion regime, the perturbation $q(x,t)$ will increase exponentially, and the steady-state solution will have inherent instability in the anomalous dispersion region.

We can obtain the gain of perturbation $q(x,t)$ power law growth, *i.e.*, $G(b(2)) = Im(b_1) = |b_2| \sqrt{-\frac{2\beta}{k} b_2^2 + \frac{6P_0(\eta_1 + \eta_2) + 10P_0^2(\eta_3 + \eta_4)}{k\alpha^2}}$, when $\beta(3P_0(\eta_1 + \eta_2) + 5P_0^2(\eta_3 + \eta_4)) < 0$. When the dispersion $\beta = -5ps^2/\text{km}$, the initial power $P_0 = 0.5W$, the nonlinearity coefficient $k = 1$, $\eta_1 = -2$, $\eta_2 = -2$, $\eta_3 = -2$, and $\eta_4 = -2$, the gain spectrum function graph of modulation instability is as follows:

In Figure 15, we can see that the gain spectrum $G(b_2)$ is symmetric about $b_2 = 0$, and the maximum value of the gain spectrum is related to the dispersion β, the initial power P_0, and the fractional-order α.

4 Conclusion

In this work, we mainly focus on the generalized coupled fractional nonlinear Helmholtz equation with cubic and quintic nonlinear effects in fiber optic propagation. In order to understand the dynamic behavior of the equation, through processes such as fractional derivatives, traveling wave transformations, and linear transformations, the equation is transformed into a two-dimensional planar dynamical system. Then through qualitative analysis, including phase portrait and bifurcation, parameter sensitivity analysis, the dynamic behavior of the system is comprehensively revealed. Meanwhile, considering that the

stability of the system may be affected by disturbances, we analyze the dynamic behavior of the system under two different types of disturbances and provide possible reasons for the changes. Finally, the conditions for the system to maintain stability are provided through modulation instability. Due to the fact that the original equation is a fractional-order partial differential equation, the degree of its nonlinear terms is relatively high, reaching three and five degrees. Under the interaction between the nonlinear and dispersion terms, light waves produce self-modulation and self-steeping effects. When the interaction between the nonlinear and dispersion terms reaches equilibrium, optical solitons can be formed. Meanwhile, this interaction inevitably leads to modulation of the steady state, resulting in modulation instability. The study of modulation instability not only helps to deepen the understanding of the essence of nonlinear optical phenomena, but also provides new technological means and solutions for fields such as fiber optic communication and optical information processing. When we make a series of transformations to the system, we may overlook some of the effects, but such processing is a necessary means of analysis. In future research, different methods can be considered and comparative analysis can be conducted.

Acknowledgments: The authors thank Key Laboratory of Pattern Recognition and Intelligent Information Processing of Sichuan, Chengdu University, Chengdu, China (Grant No. MSSB-2024-07) and funding of V.C. & V.R. Key Lab of Sichuan Provence (Grant No. SCVCVR2024.08VS) for supporting this work.

Funding information: This work was supported by Key Laboratory of Pattern Recognition and Intelligent Information Processing of Sichuan (Grant No. MSSB-2024-07), Chengdu University, Chengdu, China. This study was supported by funding of V.C. and V.R. Key Lab of Sichuan Provence (Grant No. SCVCVR2024.08VS).

Author contributions: All authors have accepted responsibility for the entire content of this manuscript and approved its submission.

Conflict of interest: The authors state no conflict of interest.

Data availability statement: The datasets generated and/or analyzed during the current study are available from the corresponding author on reasonable request.

References

[1] Joshi MP, Bhosale S, Vyawahare VA. Comparative study of integer-order and fractional-order artificial neural networks: Application for mathematical function generation. e-Prime-Adv Electr Eng Electr Energy. 2024;8:100601.
[2] Uddin M, Ullah Jan H, Usman M. RBF-PS method for approximation and eventual periodicity of fractional and integer type KdV equations. Partial Differ Equ Appl Math. 2022;5:100288.
[3] Yan S, Jiang D, Cui Y, Zhang H, Li L, Jiang J. A fractional-order hyperchaotic system that is period in integer-order case and its application in a novel high-quality color image encryption algorithm. Chaos Solitons Fractals. 2024;182:114793.
[4] Arimi HJ, Eslami M, Ansari A. Numerical study of distributed-order Bessel fractional derivative with application to Euler-Poisson-Darboux equation. Commun Nonl Sci Numer Simulat. 2024;133:107950.
[5] Ruggieri M, Speciale MP. Asymptotic expansion method with respect to a small parameter for fractional differential equations with Riemann–Liouville derivate. Commun Nonl Sci Numer Simulat. 2024;138:108234.
[6] Swati S, Nilam. Fractional order model using Caputo fractional derivative to analyse the effects of social media on mental health during Covid-19. Alexandr Eng J. 2024;92:336–45.
[7] MacDonald CL, Bhattacharya N, Sprouse BP, Silva GA. Efficient computation of the Grünwald–Letnikov fractional diffusion derivative using adaptive time step memory. J Comput Phys. 2015;297:221–36.
[8] Fareed AF, Semary MS, Hassan HN. An approximate solution of fractional-order Riccati equations based on controlled Picardas method with Atangana's fractional derivative. Alexandr Eng J. 2022;61:3673–8.
[9] Liu Y, Yang J, Liu Z, Xu Q. Meshfree methods for the time fractional Navier–Stokes equations. Eng Anal Boundary Elements. 2024;166:105823.
[10] Hao J, Li M. A new class of fractional Navier–Stokes system coupled with multivalued boundary conditions. Commun Nonl Sci Numer Simulat. 2024;136:108098.
[11] Chen J, Li X, Shao Y. Numerical analysis of fractional-order Black–Scholes option pricing model with band equation method. J Comput Appl Math. 2024;451:115998.
[12] Zhao T, Zhao L. Jacobian spectral collocation method for spatio-temporal coupled Fokker–Planck equation with variable-order fractional derivative. Commun Nonl Sci Numer Simulat. 2023;124:107305.
[13] Faridi WA, A-M Wazwaz, Mostafa AM, Myrzakulov R, Umurzakhova Z. The Lie point symmetry criteria and formation of exact analytical solutions for Kairat-II equation: Paul-Painlevé approach. Chaos Solitons Fractals. 2024;182:114745.
[14] Azar EA, Jalili B, Azar AA, Jalili P, Atazadeh M, Ganji DD An exact analytical solution of the Emden-Chandrasekhar equation for self-gravitating isothermal gas spheres in the theory of stellar structures. Phys Dark Univ. 2023;42:101309.
[15] Mahor TC, Mishra R, Jain R. Analytical solutions of linear fractional partial differential equations using fractional Fourier transform. J Comput Appl Math. 2021;385:113202.
[16] Abd Elbary FE, Ali KK, Semary MS. A new approach for solving fractional Kundu-Eckhaus equation and fractional massive Thirring

model using controlled Picardas technique with ρ-Laplace transform. Partial Differ Equ Appl Math. 2024;10:100675.
[17] Khabiri A, Asgari A, Taghipour R. Analysis of fractional Euler-Bernoulli bending beams using Greenas function method. Alexandr Eng J. 2024;1060:312–27.
[18] Mohamed MZ, Elzaki TM. Applications of new integral transform for linear and nonlinear fractional partial differential equations. J King Saud Univ-Sci. 2020;32:544–9.
[19] Ghanim F, Khan FS, Al-Janaby HF, Ali AH. A new hybrid special function class and numerical technique for multi-order fractional differential equations. Alexandr Eng J. 2024;104:603–13.
[20] Agrawal K, Kumar S, Alkahtani BS, Alzaid SS. A numerical study on fractional-order financial system with chaotic and Lyapunov stability analysis. Results Phys. 2024;60:107685.
[21] Wang H, Wang J, Zhang S, Zhang Y. A time splitting Chebyshev-Fourier spectral method for the time-dependent rotating nonlocal Schrödinger equation in polar coordinates. J Computat Phys. 2024;498:112680.
[22] Carbonaro A, Dragicević O. On semigroup maximal operators associated with divergence-form operators with complex coefficients. J Differ Equ. 2024;394:98–119.
[23] Qing L, Li X. Meshless analysis of fractional diffusion-wave equations by generalized finite difference method. Appl Math Lett. 2024;157:109204.
[24] Akrami MH, Poya A, Zirak MA. Solving the general form of the fractional Black–Scholes with two assets through reconstruction variational iteration method. Results Appl Math. 2024;22:100444.
[25] Huang Y, Rad NT, Skandari MH, Tohidi E. A spectral collocation scheme for solving nonlinear delay distributed-order fractional equations. J Comput Appl Math. 2024;456:116227.
[26] Li Z, Zhao S. Bifurcation, chaotic behavior and solitary wave solutions for the Akbota equation. AIMS Math. 2024;9:22590–601.
[27] Fukui T, Li Q Pei D. Bifurcation model for nonlinear equations. Hokkaido Math J. 2024;53(2):349–75.
[28] Zhang K, Li Z. Bifurcation, chaotic pattern and optical soliton solutions of generalized nonlinear Schrödinger equation. Results Phys. 2023;51:106721.
[29] Nasreen N, Muhammad J, Jhangeer A. Dynamics of fractional optical solitary waves to the cubic–quintic coupled nonlinear Helmholtz equation. Partial Differ Equ Appl Math. 2024;11:100812.
[30] Alsaud H, Youssoufa M, Inc M, Inan IE, Bicer H. Some optical solitons and modulation instability analysis of (3+1)-dimensional nonlinear Schrödinger and coupled nonlinear Helmholtz equations. Opt Quantum Electron. 2024;56:1138.
[31] Atangana A, Baleanu D, Alsaedi A. Analysis of time-fractional Hunter-Saxton equation: a model of neumatic liquid crystal. Open Phys. 2016;14:145–9.
[32] Chen T, Huang L, Yu P. Center condition and bifurcation of limit cycles for quadratic switching systems with a nilpotent equilibrium point. J Differ Equ. 2021;303:326–68.